npg

Wentilactone A as a novel potential antitumor agent induces apoptosis and G2/M arrest of human lung carcinoma cells, and is mediated by HRas-GTP accumulation to excessively activate the Ras/Raf/ERK/p53-p21 pathway

C Lv[1,5], Y Hong[2,5], L Miao[3,5], C Li[4], G Xu[4], S Wei[1], B Wang*[,4], C Huang*[,1] and B Jiao*[,1]

Chemotherapy remains the common therapeutic for patients with lung cancer. Novel, selective antitumor agents are pressingly needed. This study is the first to investigate a different, however, effective antitumor drug candidate Wentilactone A (WA) for its development as a novel agent. In NCI-H460 and NCI-H446 cell lines, WA triggered G2/M phase arrest and mitochondrial-related apoptosis, accompanying the accumulation of reactive oxygen species (ROS). It also induced activation of mitogen-activated protein kinase and p53 and increased expression of p21. When we pre-treated cells with ERK, JNK, p38, p53 inhibitor or NAC followed by WA treatment, only ERK and p53 inhibitors blocked WA-induced apoptosis and G2/M arrest. We further observed Ras (HRas, KRas and NRas) and Raf activation, and found that WA treatment increased HRas–Raf activation. Knockdown of HRas by using small interfering RNA (siRNA) abolished WA-induced apoptosis and G2/M arrest. HRas siRNA also halted Raf, ERK, p53 activation and p21 accumulation. Molecular docking analysis suggested that WA could bind to HRas-GTP, causing accumulation of Ras-GTP and excessive activation of Raf/ERK/p53-p21. The direct binding affinity was confirmed by surface plasmon resonance (SPR). In vivo, WA suppressed tumor growth without adverse toxicity and presented the same mechanism as that in vitro. Taken together, these findings suggest WA as a promising novel, potent and selective antitumor drug candidate for lung cancer.

Lung cancer is the leading cause of cancer-related deaths worldwide.[1] There are two main types of lung cancers, non-small-cell lung cancer (NSCLC) and small-cell lung cancer (SCLC). NSCLC is the common type of lung cancer and constitutes about 80% of all lung cancer cases. Although surgery is the only curative treatment of NSCLC, fewer than 20% of tumors can be radically resected.[2] SCLC is less common and accounts for 20% of cases, but as this type of lung cancer grows quickly and is likely to spread, it is more difficult to cure by surgical resection.[3] Therefore, chemotherapy remains common for patients with NSCLC or SCLC.[4] Although systemic chemotherapy has been reducing the lung cancer mortality, both dose-limiting toxicity and poor disease progression remain inevitable.[5] In recent decades, newly effective therapeutic treatments or novel compounds that can target certain molecular pathways used in the multistep carcinogenesis process of NSCLC have been explored; however, not for SCLC.[6,7]

The Ras family, containing H-(or Ha-) Ras, K-(or Ki-) Ras and N-Ras, is commonly considered to be oncogenes; the Ras/Raf/ERK pathway is thought to be functional downstream of the epidermal growth-factor receptor (EGFR), which has been associated with a more aggressive disease or poor prognosis in a variety of cancer systems including lung

[1]Department of Biochemistry and Molecular Biology, Second Military Medical University, Shanghai 200433, China; [2]Teaching and Research Office of Chinese Materia Medica, College of Pharmaceutical Sciences, Zhejiang Chinese Medical University, Hangzhou, Zhejiang 310052, China; [3]Department of Pharmacology, School of Pharmacy and Institute of Biomedical Sciences, Fudan University, Shanghai 200032, China and [4]Key Laboratory of Experimental Marine Biology, Institute of Oceanology, Chinese Academy of Sciences, Qingdao 266071, China
*Corresponding authors: B Wang, Key Laboratory of Experimental Marine Biology, Institute of Oceanology, Chinese Academy of Sciences, 7 Nanhai Road, Qingdao 266071, China. Tel: +86 0532 82898553; Fax: +86 0532 82898612; E-mail: wangbingui@gmail.com
or C Huang, Department of Biochemistry and Molecular Biology, Second Military Medical University, Xiangyin Road No. 800, Yangpu District, Shanghai 200433, China. Tel: +86 21 81870970 8002; Fax: +86 21 65334333; E-mail: huangcaiguo@hotmail.com
or B Jiao, Faculty of Basic Medicine, Second Military Medical University, Xiangyin Road No. 800, Yangpu District, Shanghai 200433, China. Tel: +86 21 81870970 8001; Fax: +86 21 65334333; E-mail: jiaobh@live.cn
[5]These authors contributed equally to this work.

cancer.[8] However, it is now clear that oncogenic Ras can also deregulate apoptosis. There has been an increasing appreciation that Ras, and other oncogenes, paradoxically induce both pro- and anti-apoptotic signaling. The ultimate outcome of these contradictory signals depends greatly on the cell type and environment. Throughout the past 10–15 years, reports have suggested that activation of Ras proteins can have detrimental effects on mammalian cells, ultimately leading to death by apoptosis or other mechanisms.[9] Furthermore, activation of Raf and/or ERK has been observed to increase cell death in studies of commonly used chemotherapy agents, for example, cis-diamminedichloroplatinum (II) (cisplatin),[10] paclitaxel[11] and etoposide.[12] Furthermore, combining chemotherapy with EGFR inhibitors in NSCLC has not produced a survival advantage. Therefore, the molecular mechanism of anticancer agents interacting with the Ras/Raf/ERK pathway is still unclear; clarifying it could lead to the identification of new molecular targets that might be manipulated to trigger cell death in cancer cells.

We have reported that a series of tetranorditerpenoids including asperolides A–C, Wentilactones A and B isolated from a marine-derived endophytic fungus, Aspergillus wentii EN-48, have cytotoxic activities against various human tumor cell lines.[13–15] We report here that EN-48-56, known as Wentilactone A (WA), exerts a significantly inhibitory effect on the lung carcinoma cell lines NCI-H460 and NCI-H446 without markedly inhibiting the proliferation of normal HUVECs. Furthermore, WA has the opposite molecular mechanism to EGFR inhibitors. It directly targets HRas-GTP and excessively activates the Ras/Raf/ERK pathway, which initiates apoptosis and G2/M phase arrest via p53-p21 participation and stabilization. In vivo, WA is also effective in inhibition of tumor xenograft growth and is safer than cisplatin. All of these present the potential use of WA to treat NSCLC and SCLC.

Results

WA inhibits cell proliferation and colony formation in NCI-H460 and NCI-H446 cells.
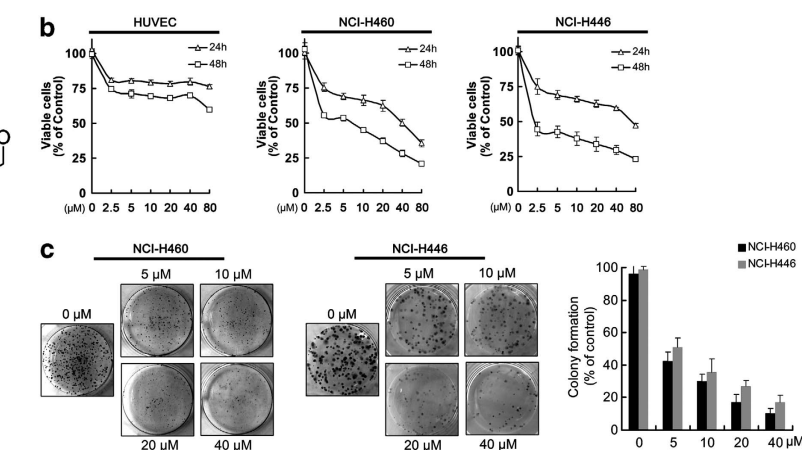
As shown in Figure 1b, WA inhibited cell growth in both cancer cell lines in a dose-dependent manner. The IC_{50} value of WA toward NCI-H460 cell viability was $5.56 \pm 0.89 \mu M$, and that toward NCI-H446s was $1.90 \pm 1.30 \mu M$ after 48 h. However, WA did not show markedly inhibition of HUVECs. Additional clonogenic assays also indicated that WA suppressed the ability of a single-carcinoma cell growth into a colony. Clonogenicity of both cancer cell lines was reduced in a concentration-dependent manner after exposure to WA (Figure 1c).

WA induces mitochondrial-related apoptosis in NCI-H460 and NCI-H446 cells.

We next assessed the effect of WA on the induction of apoptosis in NCI-H460 and NCI-H446. Apoptotic cells with nuclear condensation and fragmentation can be visualized by DAPI staining. The photographs in Figure 2a show the results of 48 h treatment with $10 \mu M$ WA. Annexin V-FITC/PI double stain was used to make a quantitative evaluation of apoptosis. Compared with the control group (0.1% DMSO), $10 \mu M$ WA triggered apoptosis of NCI-H460 and NCI-H446 cells in a time-dependent manner; $29.65 \pm 7.91\%$ and $47.34 \pm 7.36\%$ apoptosis at 48 h was induced, respectively (Figure 2a).

To investigate the mitochondrial apoptotic events involved in WA-induced apoptosis, we tested the changes of the mitochondrial membrane potential ($\Delta\Psi m$), bcl-2 family proteins, cytochrome c release, proteolytic cleavage of procaspase and the effect of a general caspase inhibitor (z-VAD-fmk). The loss of $\Delta\Psi m$, which was measured by JC-1, can be tested after exposure of cells to $10 \mu M$ WA in both cells, especially in NCI-H446 cells (Figure 2b). To further confirm whether WA-induced cell apoptotic death was caspase dependent, a general caspase inhibitor, z-VAD-fmk, was used. As indicated in Figure 2c, the addition of z-VAD-fmk reduced the apoptotic response from 27.89 to 10.73% in NCI-H460 cells and from 54.79 to 10.32% in NCI-H446 cells after 48 h. Immunoblot analysis showed that treatment of NCI-H460 and NCI-H446 cells with $10 \mu M$ WA increased bax and bad protein levels and, in contrast, decreased bcl-2 and Mcl-1 levels in a time-dependent manner. Consistently, cytochrome c was released and cleavage of procaspase-3/7 and

Figure 1 The effects of Wentilactone A (WA) on cell growth inhibition and colony formation. (**a**) Chemical structure of Wentilactone A. (**b**) HUVEC and human lung carcinoma cells (NCI-H460 and NCI-H446 cells) were treated with 0, 2.5, 5, 10, 20, 40, 80 μM of WA for 24 and 48 h, respectively. Cell viability was detected by MTT assay. (**c**) Effect of WA on the number of colony-forming cells as evaluated by clonogenic assay. Colonies were stained with trypan blue. Values are means ± S.D. from three independent experiments
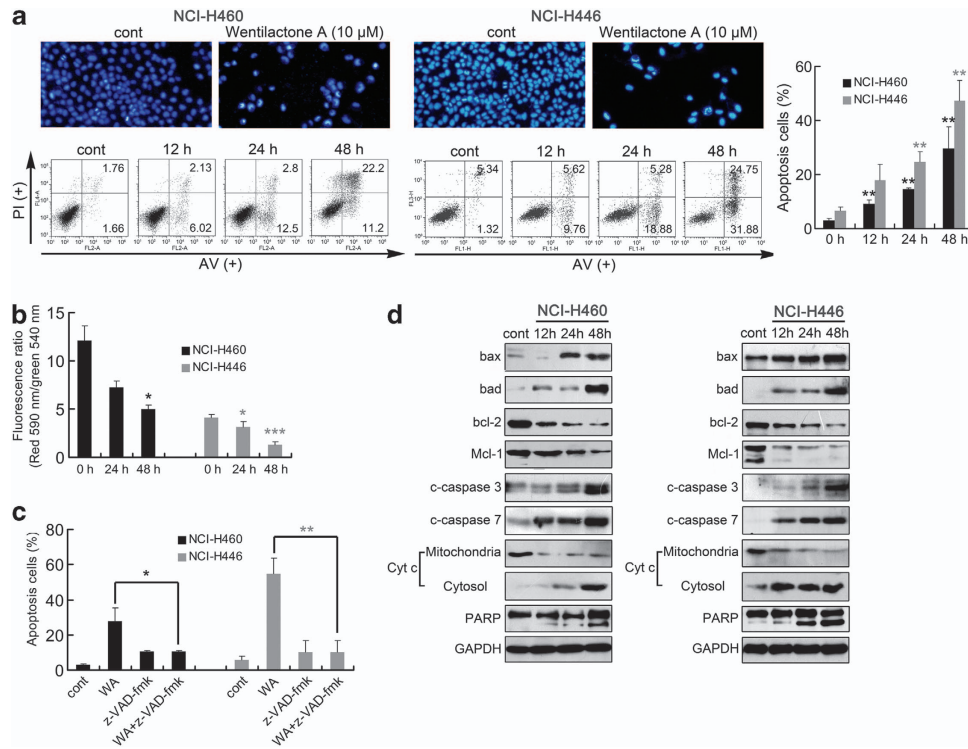
Figure 2 WA triggers mitochondrial-related apoptosis in NCI-H460 and NCI-H446 cells. (**a**) WA-induced morphological changes as indicated by DAPI staining. Representative photomicrographs of control and 48 h 10 μM WA treatment groups are showed. Apoptosis in NCI-H460 and NCI-H446 cells was assessed after 12–48 h of treatment with 10 μM WA by Annexin V-FITC/PI binding and measured by flow-cytometry analysis. Numbers indicate the percentage of cells in each quadrant. **$P < 0.01$ *versus* the drug-untreated group. (**b**) The mitochondrial membrane potential was measured using JC-1 by flow cytometry. Decrease in the ratio of the green fluorescence (FITC) to the red fluorescence (PE) indicates loss of $\Delta\Psi$m. (**c**) NCI-H460 and NCI-H446 cells were treated with 20 μM z-VAD-fmk, a caspase inhibitor, for 1 h before treatment with 10 μM WA for 48 h. Apoptosis was assessed by flow cytometry as mentioned above. *$P < 0.05$, **$P < 0.01$. (**d**) Western blot of cells analyzed for bax, bad, bcl-2, Mcl-1, cleaved caspase-3/7, PARP, cytochrome *c* in cytosol and mitochondria after treatment with 10 μM WA for the indicated time periods. Results are representative of three separate experiments. GPDH is shown as protein-loading control

PARP was also observed (Figure 2d), indicating activation of the intrinsic apoptosis pathway in WA-induced cell death.

WA induces G2/M arrest. In order to examine whether cell-cycle disturbance is responsible for WA-mediated cell growth inhibition, cell-cycle distribution and related checkpoint factors were studied. Cells were treated with 10 μM WA for 24 and 48 h, respectively. The results showed that WA-treated cells accumulated progressively in the G2/M phase (Figure 3a). Compared with the control, treatment with WA for 48 h resulted in an increased proportion of G2/M phase in NCI-H460 cells from 10.44% (control) to 29.34% (48 h, WA) and from 5.43% (control) to 13.16% (48 h, WA) in NCI-H446 cells, about a 3-fold and 2.5-fold increase, respectively. Besides, WA treatment resulted in a time-dependent decrease in the protein expression of cyclin B1, cdc2, p-cdc2, cdc25C and p-cdc25C (Figure 3b). Contrary to the expectation, protein levels of p-cdc25C (Ser216) and p-cdc2 (Tyr15) were decreased after WA treatment, which might be caused by the drastic decrease in the total expression of cdc25C and cdc2. All the above suggest that G2/M phase arrest also accounts for the antiproliferative effect of WA in both cells and more significantly in NCI-H460 cells.

ERK and p53 regulate WA-induced apoptosis and G2/M arrest. Mitogen-activated protein kinase (MAPK) signaling

cascades have been proved to have essential roles in the regulation of a wide variety of cellular processes, including cell growth, migration, proliferation, differentiation, development, apoptosis and cell growth arrest.[16] To further investigate the possible mechanism of WA, the activations of ERK, JNK and p38 MAP kinases were determined in both cell lines. Immunoblot showed that the phosphorylations of ERK, p38 and JNK were significantly increased after WA treatment (Figure 4a), and pre-treatment with 20 μM PD98059, SB203580 or SP600125 almost completely blocked phosphorylation of ERK, p38 or JNK (Figure 4b). However, only ERK inhibitor PD98059 significantly inhibited WA-induced apoptosis and G2/M arrest, and brought apoptosis-related and G2/M regulatory proteins to normal levels. There was no significant difference between the WA-treatment group and the JNK or p38 inhibitor pre-treatment group (Figure 4c). Considering that p53, which is a critical determinant in controlling both cell-cycle arrest and apoptosis,[17,18] usually has crosstalk with MAPKs,[19] and the downstream regulator p21 is probably involved in G2/M arrest through the p53-dependent pathway,[20] we detected p53 and p21 protein levels using western blot analysis. The data showed that WA treatment caused a marked time-dependent increase in the phosphorylation status of p53 and in the level of p21 protein (Figure 4d). Then the role of p53 in WA-induced apoptosis and G2/M arrest was studied. Cells
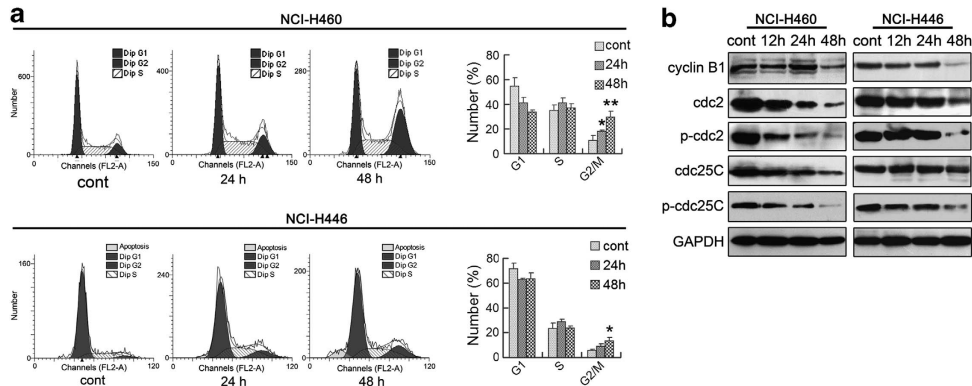
Figure 3 WA induces cell-cycle arrest in NCI-H460 and NCI-H446 cells. (**a**) Cells were treated with or without 10 μM WA for the indicated time periods and then the cell-cycle distribution was measured using flow cytometry. The percentage of cells in each population was shown as mean $\pm$ S.D. from three independent experiments. *$P < 0.05$, **$P < 0.01$. (**b**) Western blot analysis of G2/M transition-related proteins after WA treatment
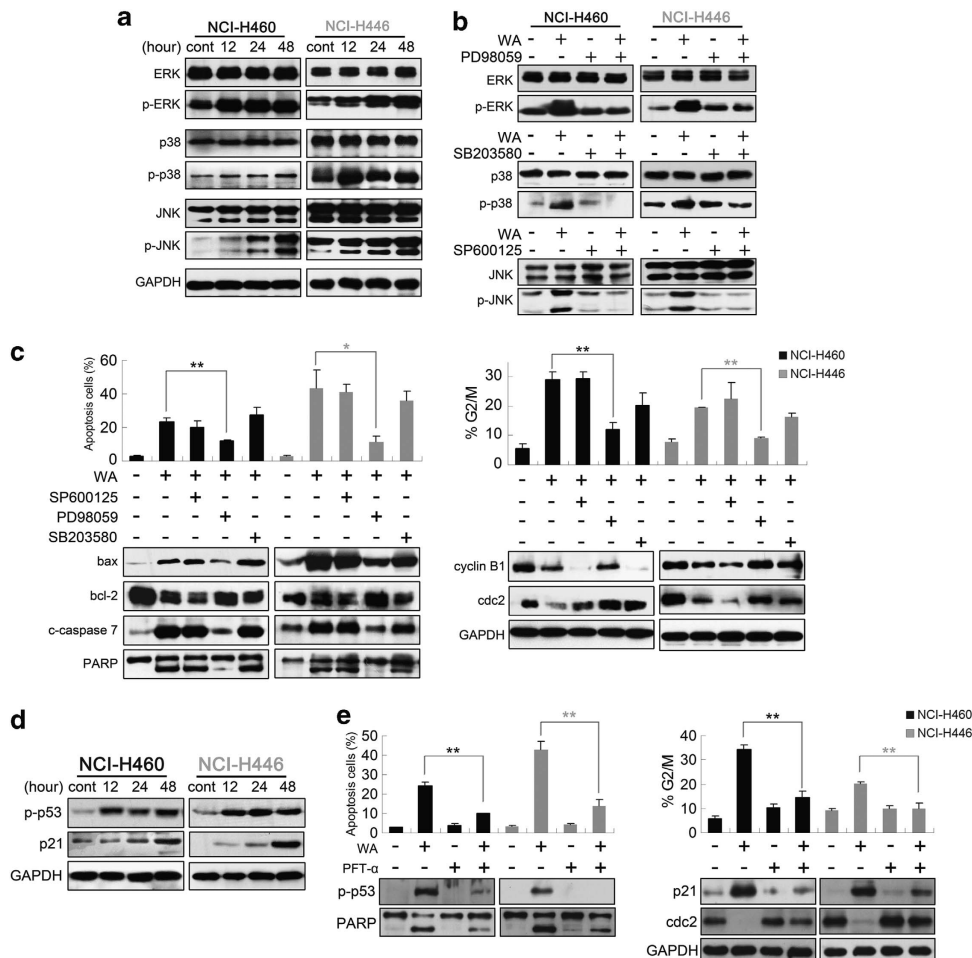

Figure 4 ERK and p53 regulate WA-induced apoptosis and G2/M arrest. (**a**) Cells were treated with 10 μM WA for various incubation times, total and phosphorylated MAPK members (JNK, p38, ERK) were detected using immunoblot assay. (**b**) Cells were pre-treated with 20 μM MEK inhibitor (PD98059), JNK inhibitor (SP600125) or p38 inhibitor (SB203580) followed by treatment with or without 10 μM WA for 48 h. Total and activation forms of ERK, JNK or p38 were evaluated by western blotting; (**c**) Cells were pre-treated with the indicated inhibitor for 1 h, then treated with 10 μM WA for 48 h and analyzed for apoptosis, cell-cycle analysis and expression of bax, bcl-2, cleaved caspase-7, PARP, cyclin B1 and cdc2. (**d**) p-p53 (Ser 15) and p21 protein levels were detected after WA treatment. (**e**) Cells were incubated for 1 h in the presence or absence of PFT-α (20 μM) and then 10 μM WA was added followed by incubation for an additional 48 h. The induction of apoptosis and cell-cycle distribution were determined by flow cytometry. Apoptosis and G2/M checkpoint-related proteins were detected by western blot. Values are means $\pm$ S.D. from three independent experiments. *$P < 0.05$, **$P < 0.01$

were pre-treated with 20 μM p53 inhibitor Pifithrin-α (PFT-α) for 1 h before incubating WA for a further 48 h. As shown in Figure 4e, pre-treatment with PFT-α prevented the WA-induced apoptosis and reduced the accumulation of p21 and G2/M phase cells, suggesting that WA initiated apoptosis and G2/M phase arrest via p53-p21 participation and activation. WA treatment also resulted in a marked time-dependent reactive oxygen species (ROS) accumulation (see Supplementary Material). ROS is known to be a mediator of MAPKs, SAPKs, and so on.[21] Numerous investigations have documented that following exposure to cytotoxic drugs, excessive production of ROS in cells usually induced the loss of cell function and apoptosis/necrosis.[22–24] However, in this study, ROS is not the major mediator of WA-induced cell death and growth inhibition in human lung carcinoma cells but a 'post-mitochondrial' event and fails to regulate MAPK signals (Supplementary Figure S1).[25,26]

WA induces cell-cycle arrest and apoptosis through a Ras/Raf/ERK/p53-p21-dependent pathway. As described

above, it is essential to check whether Ras, a common activator of the ERK signaling pathway, is involved in WA's toxic effect on NCI-H460 and NCI-H446 cells. The activation of Ras was tested by precipitating the GTP-bound forms of Ras using the Ras-binding domain (RBD) of Raf-1 as an activation-specific probe.[27] As observed in Figure 5a, WA treatment did not alter the expression level of total Ras; KRas-GTP of NCI-H446 cells and NRas-GTP in both cells were almost not observed; and because of an activating mutation of KRas (Q61H) in NCI-H460 cells, numerous activated forms of KRas were detected; however, no obvious changes of KRas-GTP were observed after the WA treatment. WA only induced the activation of HRas in both cells, and the phospho-c-Raf (p-c-Raf) presented consistent changes with HRas-GTP (Figure 5a).

To investigate whether Ras is responsible for WA-induced cell death or growth inhibition, we used small interfering RNA (siRNA) to knock down HRas, and observed that WA-induced apoptosis and G2/M arrest in both cells were significantly abolished (Figure 5b).
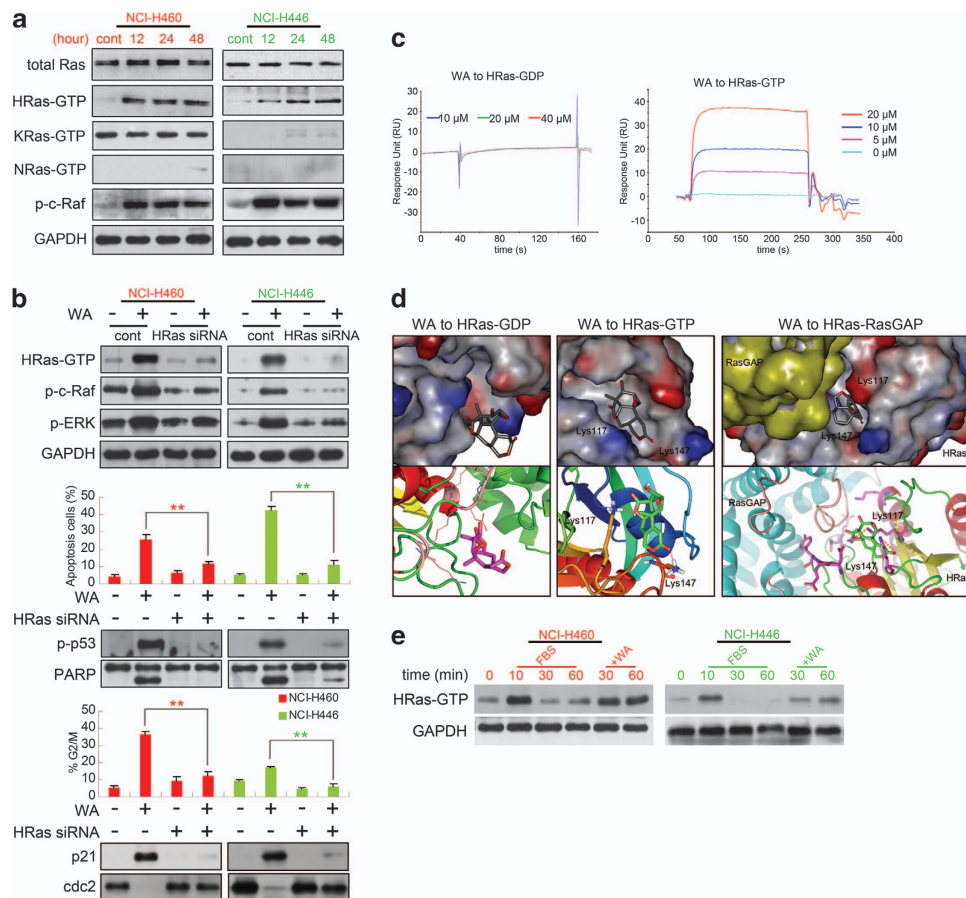

Figure 5 WA targets HRas to activate the Ras/Raf/ERK/p53-p21 pathway. (**a**) Total Ras, HRas-GTP, KRas-GTP, NRas-GTP and p-c-Raf (Ser338) protein levels were increased in both cells after 10 μM WA treatment. (**b**) Cells transfected with HRas siRNA or not were treated with or without 10 μM WA for 48 h, then cells were harvested for western blot assay against HRas-GTP, p-c-Raf, p-ERK. Apoptosis, cell-cycle analysis and related-proteins were also detected at 48 h. Values were means ± S.D. of three independent experiments. *$P < 0.05$, **$P < 0.01$ versus control groups. (**c**) Binding affinity of WA to the HRas-GDP and HRas-GTP proteins determined by SPR. (**d**) 3D structure of interaction between WA and HRas-GDP (left), HRas-GTP (middle) or HRas-RasGAP (right) in detail. WA is represented by the stick model. Hydrogen bond was signed in red. (**e**) Starved cells were stimulated with 10% FBS or incubated with WA after 10 min FBS stimulation for the indicated time points. HRas-GTP levels were monitored using immunoblot assay

6

In addition, HRas siRNA brought p-c-Raf, p-ERK, p-p53, p21, PARP and cdc2 expressions to normal levels (Figure 5b).

The results achieved above led us to consider whether HRas is the potent target of WA. Thus, surface plasmon resonance (SPR) biosensor analysis was used to test direct binding of WA to HRas-GTP/GDP protein, and the binding affinity of WA to the proteins was reflected by response unit (RU) values. The binding between WA and HRas-GDP showed no response (Figure 5c left), while WA binding to HRas-GTP presented a significant and dose-dependent increase in response unit with $K_D = 15.7\,\mu$M (Figure 5c right), indicating that WA may have a specific binding affinity toward Ras-GTP. But how does this binding induce HRas-GTP accumulation? We further employed molecular docking to investigate WA-HRas interaction at the atomic level. The 3D structural model of Ras-GTP was obtained from the Protein Data Bank (PDB ID: 4DLR). As shown in Figure 5d, WA located at the GTP-binding site through hydroxyl oxygen atoms forming two O-H hydrogen bonds with the HRas-GTP residues Lys117 and Lys147, and the binding energy was -145.53 kcal/mol (middle); as for HRas-GDP (PDB ID: 3KUD), WA could also enter the GDP-bingding cavity, but no hydrogen bonds could be formed (left). These docking results confirmed the former SPR analysis. In addition, Lys117 and Lys147 were just the two residues on the interface binding pocket of HRas with Ras-specific GTPase activating proteins (RasGAPs, or GAPs), and GAPs, which supply additional catalytic residues ('arginine finger') such that a water molecule is optimally positioned for a nucleophilic attack on the gamma phosphate of GTP, hydrolyze a bound GTP molecule into GDP.[28] Therefore, referring to the HRas-RasGAP interaction (PDB ID: 1WQ1, Figure 5d right), WA forming hydrogen bonds with Lys117 and Lys147 residues might interfere with RasGAP to convert Ras-GTP into GDP-bound form, which might induce Ras-GTP accumulation. Finally, this model was confirmed by using fetal bovine serum (FBS) stimulation. When cells were serum starved for 24 h and then stimulated with FBS, HRas was rapidly activated; HRas activation reached a maximum after 10 min (Figure 5e lane 2) and returned close to the pre-stimulation level within 30 min (Figure 5e and lane 3). When WA was added after 10 min of FBS stimulation, we observed that HRas-GTP no longer returned to pre-stimulation level and remained in continuous active form (Figure 5e, lanes 5 and 6). This *in vitro* model further confirmed the docking results that WA might enter the HRas-RasGAP complex to interfere with the interaction of HRas-GTP and RasGAP.

Collectively, these results suggest that WA led HRas-GTP accumulation to excessively activate the Ras/Raf/ERK/p53-p21 pathway, which induced apoptosis and G2/M arrest of human lung carcinoma cells.

WA inhibits tumor xenograft growth. The injected carcinoma cells grew into palpable tumors in the nude mice within 4 days (Figure 6a). Cyclophosphamide-treated mice (20 mg/kg per day) or cisplatin-treated mice (2.5 mg/kg) were used as positive control to assess the effect and toxicity of WA. In mice treated with vehicle (1% DMSO in PBS) only, the tumors grew exponentially. However, the tumor growth

in mice treated with WA (2.5, 5, or 10 mg/kg per day) was dose-dependently slowed. Tumor volume was significantly reduced during WA treatment (Figures 6c and cc). The inhibitory rates at the 20th day of the 2.5, 5 and 10 mg/kg WA treatment groups of NCI-H460 xenograft-bearing mice were 48.71%, 85.11% and 95.58%, respectively (Figure 6b); as for the NCI-H446 xenograft-bearing mice, inhibitory rates were 33.78%, 80.84% and 87.12%, respectively (Figure 6bb). It should be noted that compared with the more effective Cisplatin-positive control of the two models (inhibition rates of 88.76% and 91.90%, respectively), 10 mg/kg WA treatment showed equivalent effect and weight gain during the course of therapy; however, significant weight loss was found in the cisplatin-treated animals (Figures 6d and dd).

In addition, immunohistochemical staining showed significant increase of active caspase-3 and decrease of cdc2 expression in tumors of the WA-treated mice (Figures 6f and ff), which was in accordance with the cell death and growth inhibition results obtained from the *in vitro* analyses. Increase in p-ERK and HRas-GTP (Figure 6f and ff) was also observed, indicating the same cell signaling mechanism as that *in vitro*. Furthermore, protein expression account was similar between the 10 mg/kg WA-treatment group and 2.5 mg/kg cisplatin group.

Discussion

In our study, WA significantly suppressed tumor cell growth *in vivo* and *in vitro*. It induced G2/M phase arrest and mitochondrial-related apoptosis via the Ras/Raf/ERK/p53-p21 signaling pathway (Figure 7).

Tumor suppressor p53 is a short half-life regulator. The function of p53 is achieved by increased expression at the transcriptional level and post-translational stabilization to escape ubiquitin-dependent degradation.[29,30] Phosphorylation of p53 at serine 15 and 46 sites is the main post-translational modification that is regulated by several different protein kinases, including ataxia-telangiectasia-mutated kinase[31] and MAPK.[32] The way of phosphorylation depends on the types of cells and extracellular stimuli. We reported here that WA caused a significant time-dependent phosphorylation of p53 at serine 15 in both lung carcinoma cells. The increased phosphorylation and accumulation of p53 may lead to mitochondrial apoptosis by upregulating and derepressing proapoptotic members of the bcl-2 family, such as bax, bak, bad, bid, puma and so on, while on the other hand downregulating and repressing antiapoptotic members, such as bcl-2, bcl-xl, Mcl-1 and so on.[33–39] Therefore, WA-induced phosphorylation and accumulation of p53 should be responsible for decreased bcl-2/Mcl-1, and increased bax/bad. In addition, p53 utilizes and increases the transcription of its downstream molecular p21 to modulate cdc2—the cyclin-dependent kinase required to enter mitosis.[18] P21 acts not only as one of the transcription targets of p53, but also as an inhibitor of cell-cycle progression through the G2/M checkpoint.[17,20] When phosphorylation of p53 was blocked by PFT-α, apoptosis and cell G2/M arrest were almost abolished, accompanied by recovery of p21 and cdc2 in both cell lines. Therefore, we conclude WA-induced apoptosis and G2 phase
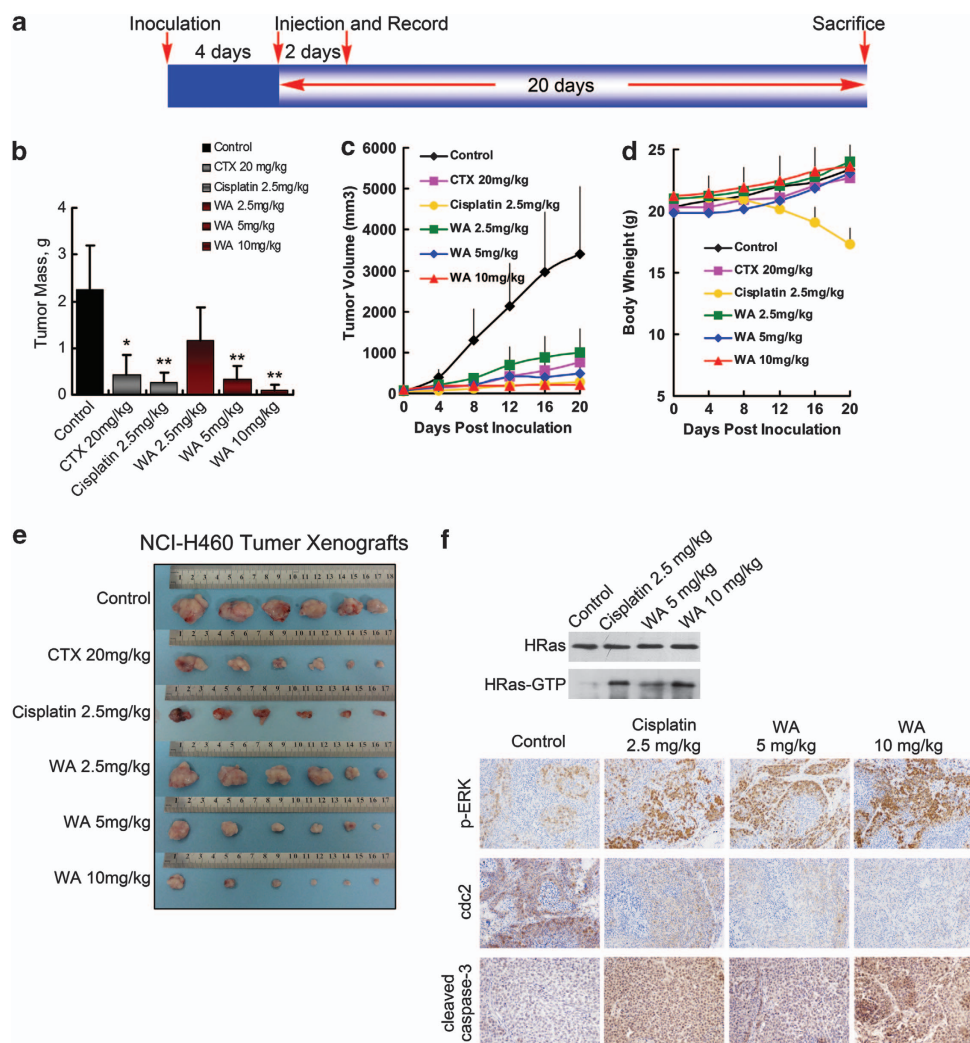
Figure 6 Effect of WA on tumor growth in xenograft models. Mice were treated with vehicle (1% DMSO) or drugs according to the protocol in panel (**a**); (**b–f**) and (**bb–ff**) are the results from NCI-H460 xenograft bearing mice and NCI-H446 xenograft bearing mice, respectively. (**b** and **bb**) Average tumor mass at sacrifice. *$P < 0.05$, **$P < 0.01$ *versus* control group. (**c** and **cc**) Transplant tumor volume after the injection. (**d** and **dd**) Body weight of nude mice. (**e** and **ee**) Tumor image from various treatment groups. (**f** and **ff**) Western blot assay for HRas, HRas-GTP and representative photomicrographs of xenograft tumor sections for IHC analysis for p-ERK, cdc2 and active caspase-3 expression ($\times 200$). Significantly increased HRas-GTP, p-ERK, active caspase-3 and decreased cdc2 expressions were observed in the WA-treated tumors compared with the vehicle control groups

arrest in human NCI-H460 and NCI-H446 lung carcinoma cells is mediated by p53-p21 stabilization.

The diverse, even opposing, effects of ERK on cell behavior have been reviewed in recent years,[40] and ERK usually has crosstalk with p53 signaling in aspects of cell autophagy and apoptosis,[41] whereas Ras protein is best known for its ability to serve as a molecular switch regulating cell growth, differentiation and survival. Gene mutations that result in expression of constitutively active forms of Ras have been linked to oncogenesis.[42] However, considerable evidence has gradually accumulated to support a paradoxical role for Ras proteins in initiation of cell death pathways.[43] Here we observed that WA induced the activation of HRas in both cells, and knockdown HRas with siRNA not only suppressed the WA-induced G2/M arrest and apoptosis, but also brought p-c-Raf, p-ERK, p-p53 and p21 to normal level, suggesting that Ras mediated Raf/ERK/p53/p21 signaling and active Ras

sent death signals to cells by WA treatment. In light of the balance and interplay of multiple signaling networks involved in various signaling contexts of different cell type and stimuli, it is not surprising that Ras/ERK regulation is complex. But we can simply explain the dual, even opposing, functions of the proteins by the notion that: ultimate growth or death is based on signal intensity and duration. It is just like there is a baseline under which cell growth capacity is in proportion to the signal intensity; if sustained and strengthened signal accumulates to overcome the baseline, growth is inversely related to signal intensity and finally converts to death.[21] Thus, under growth condition or other relatively weak stimuli toward Ras/ERK, elevated activation of Ras/ERK confers a growth advantage to tumor cells. However, exposure of these cells to damaging agents that induce prolonged substantial increase of active Ras/ERK level results in initiation of apoptosis. As in the case of our study, Ras was constantly activated. The activation
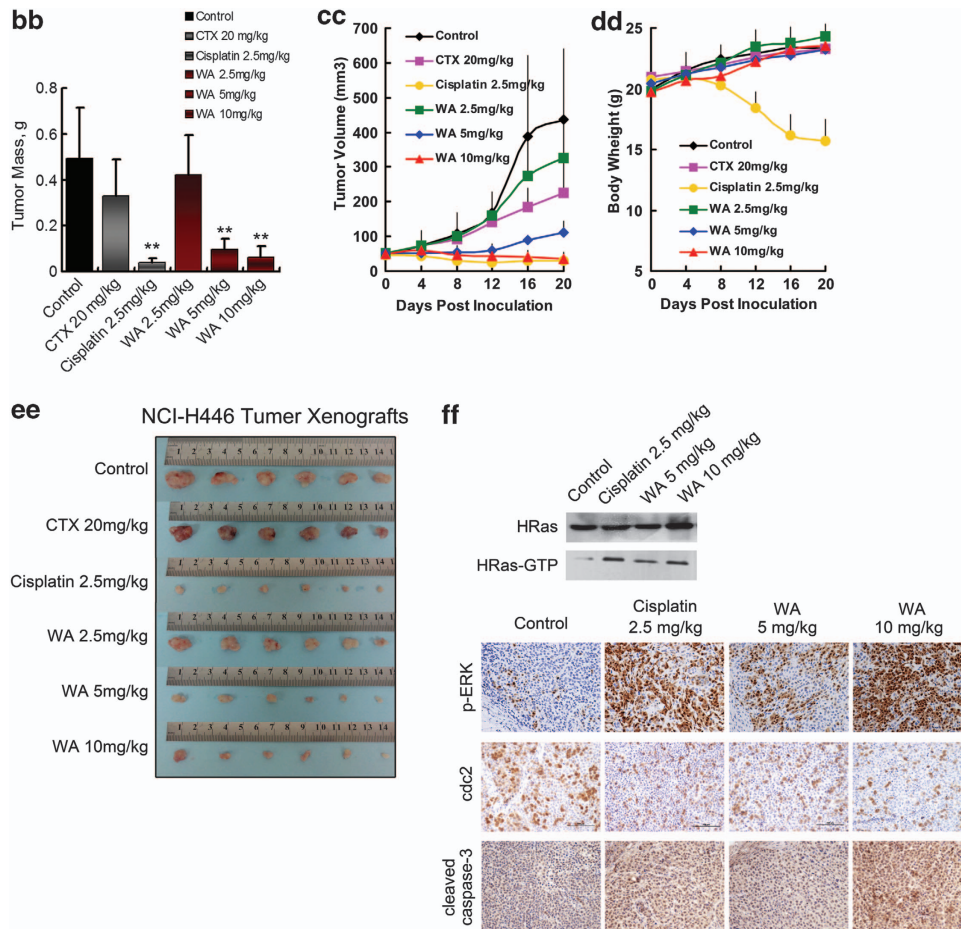
Figure 6 (Continued)

prolonged to 48 h at least, which in turn created and sent a damage signal to cells. In addition, compared to the IC$_{50}$ (5.56 ± 0.89 and $1.90 \pm 1.30\,\mu$M, respectively) and apoptosis rate ($29.65 \pm 7.91\%$ and $47.34 \pm 7.36\%$ apoptosis at 48 h, respectively) of the two lung carcinoma cells, we noticed that NCI-H446 presented more sensitivity to WA treatment than NCI-H460 cells, which is probably because NCI-H460 cells have an activating mutation in KRas (Q61H). The mutation leads to an elevated basal level/activity of Ras/Raf/ERK signaling, and higher baseline to overcome.

It is well accepted that small-molecule drugs generally exert their therapeutic functions by binding to the cavities of proteins to influence their biological activities.[44] In our study, it seemed only HRas (one of the Ras isoforms) was selectively chosen to act as the mediator of WA-induced apoptosis and G2/M arrest. Therefore, whether WA directly binded to HRas needs to be clarified. SPR analysis showed that WA might have a specific binding affinity toward HRas-GTP. Molecular docking further indicated WA could insert HRas-GTP, forming hydrogen bonds with HRas-GTP at Lys117 and Lys147 residues, which interfered with the GAP catalytic activity and then induced Ras-GTP accumulation. We know that GAPs and guanine-nucleotide-exchange factors bind to Ras proteins and regulate their activity by modulating guanine nucleotide cycling. Guanine-nucleotide-exchange factors activate Ras

by promoting exchange of GDP for GTP. Conversely, GAPs have the opposite function and lead to inactivation of Ras by facilitating hydrolysis of GTP to GDP.[45] As shown in Figure 5e, after 10% FBS stimulation, starved cells could elevate HRas-GTP levels rapidly through guanine-nucleotide-exchange factor regulation, followed by GAPs facilitating hydrolysis of GTP to GDP in a short time.[46,47] Addition of WA inhibited the return of HRas-GTP to pre-stimulation level and maintained HRas-GTP in continuous active form, which suggested that WA weakened or even eliminated the catalytic activity of GAP. This model also confirmed the molecular docking results.

In vivo, WA treatment significantly reduced tumor growth in the two models. 10 mg/kg WA treatment showed equivalent effect with 2.5 mg/kg Cisplatin. It is well known that cisplatin is a chemotherapeutic agent used in the treatment of a wide range of human malignancies, including NSCLC and SCLC. Though Cisplatin combination chemotherapy is the cornerstone of treatment of many cancers, serious adverse effects offset the productivity of treatment and renders the chemotherapy unsustainable.[48,49] As we observed in this study, significant weight loss was found in the cisplatin-treated animals. In contrast, the weight gain of WA-treated mice indicated the potential clinical benefit of WA in reduced adverse toxicity and the feasibility for upward adjustment of
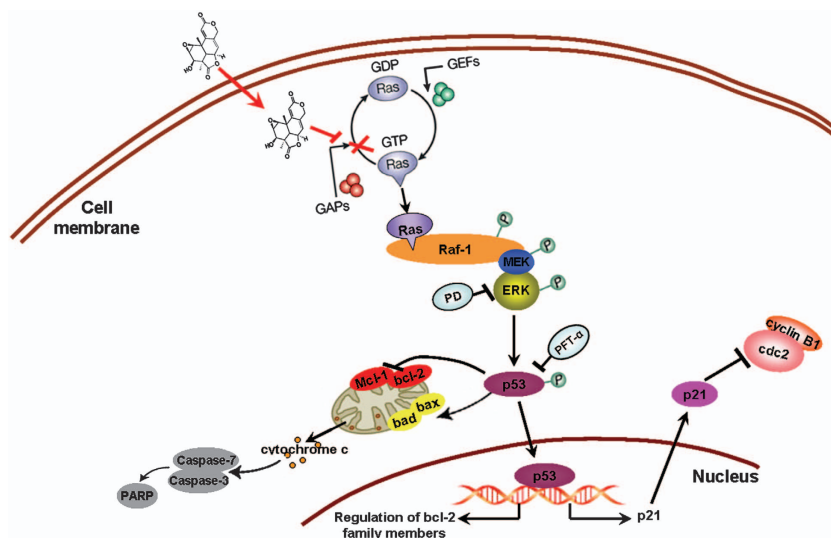
Figure 7 Overview of pathways for WA-induced apoptosis and cell-cycle arrest in NCI-H460 and NCI-H446 cells

dosage for improved treatment outcomes compared with cisplatin.

Taken together, our results demonstrate that WA directly targets HRas-GTP and excessively activates the Ras/Raf/ERK pathway, which initiates apoptosis and G2/M phase arrest via p53-p21 participation and stabilization during human lung carcinoma cell proliferation (Figure 7). Moreover, administration of WA significantly suppressed the growth of lung carcinama xenograft by inducing apoptosis and G2/M arrest via the same cell signaling pathway in the tumor cells. Our studies thus provide a rationale for the development of WA as a chemotherapeutic agent against NSCLC/SCLC in the clinical setting.

Materials and Methods

Reagents. DMEM, RPMI 1640 medium, FBS, trypsin-EDTA, penicillin and streptomycin were purchased from Biowest (Maine et Loire, France). Annexin V-FITC/PI apoptosis detection kit, DAPI, JC-1 detection kit and cell-cycle detection kit were provided by Nanjing KeyGen Biotech Co Ltd. (Nanjing, China). GAPDH was obtained from Tianjin Sungene Biotech (Tianjin, China). Rabbit polyclonal anti-active caspase-3 antibody (AB3623) for immunohistochemistry was provided by Millipore (Chemicon International, Temecula, CA, USA). Anti-GTPase HRas antibody (ab16881) was from Abcam (Hong Kong, China); K-Ras, N-Ras antibodies and H-Ras siRNA were from Santa Cruz Biotechnology Inc. (Santa Cruz, CA, USA). All the other antibodies were purchased from Cell Signaling Technology (Beverly, MA, USA). Ras activity was assessed using the Ras activation assay kit from Upstate Biotechnology (Temecula, CA, USA). z-VAD-fmk, PD98059, SP600125, SB203580 and PFT-α were bought from Beyotime Institute of Biotechnology (Nantong, Jiangsu, China). Recombinant human HRas-GDP (purify > 90%) was purchased from Cusabio Biotech Co. Ltd (Wuhan, China). Human recombinant protein Ras-GTP (purify $\geq$ 90%) was obtained from Abcam (Hong Kong, China).

Chemical preparation and cell culture. WA, isolated from a marine-derived endophytic fungus *A. wentii* EN-48,[13] was dissolved in 100% DMSO and stored at $-20\,^{\circ}$C, then diluted with cell culture media before using. The final DMSO concentration did not exceed 0.1%. Human large cell lung carcinoma cell line NCI-H460, small-cell lung cancer cell line NCI-H446 and human umbilical vein endothelial cell line HUVEC were obtained from the cell bank of the Shanghai Institute of Cell Biology (Shanghai, China). NCI-H460 and NCI-H446 cells were cultured in RPMI-1640 medium; HUVECs were

maintained in DMEM. All cells were supplemented with 10% FBS and antibiotics (100 μg/ml streptomycin and 100 U/ml penicillin) in a humidified 5% CO_2 incubator at 37 $^{\circ}$C.

Cell viability assay. Cells were seeded into 96-well plates at 4×10^4 cells/ml, incubated for 24 h, and then treated with the indicated concentrations of WA (0, 2.5, 5, 10, 20, 40 and 80 μM) for 24 and 48 h. Cell viability was determined using the MTT assay.

Clonogenic assay. NCI-H460 cells and NCI-H446 cells (500 cells/well) were seeded in six-well plates and cultured for 24 h, followed by various concentrations of WA treatment (0, 5,10, 20 and 40 μM) for 10–14 days. After washing with PBS, colonies were fixed in methanol and stained with trypan blue.

DAPI staining. Cells were fixed with 1% paraformaldehyde for 30 min at room temperature. After washing with PBS, 300 nM DAPI was added to the fixed cells for 5 min and examined by fluorescence microscopy. Apoptotic cells were identified by condensation and fragmentation of nuclei.

Cell apoptosis assay. Cell apoptosis was determined by Annexin V-FITC/PI assay. After treatment, cells were collected and resuspended with 500 μl binding buffer at a concentration of 10^6/ml cells. After adding 5 μl Annexin V-FITC, cells were mixed and incubated at room temperature in the dark for 5–15 min. To the samples was added 5 μl PI and resuspended before analysis with a FACScalibur flow cytometer. Results were calculated by using the CellQuest software.

Mitochondrial membrane potential ($\Delta\Psi$m) assay. Change of mitochondrial membrane potential ($\Delta\Psi$m) was examined by fluorescent lipophilic cationic probe JC-1. Following treatment with 10 μM WA for the indicated time points, cells were stained with JC-1. Fluorescence was monitored at wavelengths of 490 (excitation)/540 nm (emission) and 540 (excitation)/590 nm (emission) pairs. Changes in the ratio between 590 (red) and 540 nm (green) fluorescence intensities were an indicator of the mitochondrial membrane potential.

Cell-cycle analysis. Cells were harvested, washed twice with PBS, fixed in 70% ethanol and stored at 4 $^{\circ}$C overnight, then washed with PBS, incubated with RNase at 37 $^{\circ}$C for 30 min and stained with PI (1 mg/ml) in the presence of RNase A for 30 min. Cell-cycle phase analysis was performed by using a FACScalibur flow cytometer.

Western blot analysis. Cells were lysed in western blotting lysis buffer at 4 $^{\circ}$C for 30 min. After 12 000 g centrifugation for 15 min, the protein content of supernatant was quantified using a BCA protein assay kit (Beyotime Institute of

Biotechnology). Equal amounts of the protein samples were separated by SDS-PAGE, and transferred to nitrocellulose membranes using an electro-blotting apparatus (Bio-Rad, Hercules, CA, USA). Then the membranes were blocked in blocking buffer (TBST plus 5% skimmed milk), and incubated with primary antibodies overnight at 4 °C. After that the membranes were washed with TBST and incubated with horseradish peroxidase-conjugated secondary antibodies for 1.5 h at 4 °C. Protein expression was visualized using the chemoluminescence reagent (Millipore, Bedford, MA, USA) and detected on a photographic film.

Measurement of RAS activation. The activity of the Ras protein was determined by precipitating the GTP-bound forms of Ras using the RBD of Raf-1 as an activation-specific probe.[27] Cells were lysed and the cleared lysate was subjected to a RAS-GTP assay as per the manufacturer's instructions (Upstate Biotechnology, Lake Placid, NY, USA). The amount of RAS in the bound fraction was determined by western blot analysis with the anti-Ras antibody.

siRNA transfection. Cells were plated in six-well plates at 1.5×10^5 cells/well, grown for 24 h, then transfected with 100 pmol of siRNA for 6 h using Lipofectamine 2000 reagent and OPTIMEM reduced serum medium (Invitrogen, Carlsbad, CA, USA). The cells were assayed 48 h after transfection.

SPR biosensor analysis. SPR biosensor analysis was used to verify the binding of WA to Ras-GDP/GTP protein, which was analyzed by the Center for Bio-information Technology, Chinese Academy of Sciences Shanghai, using an SPR-based Biacore 3000 instrument. In brief, the protein was immobilized on a CM5 sensor chip in 7000 response units (RU) according to the standard primary amine-coupling procedures, the immobilization buffer and the running buffer was 2% DMSO in PBS. Equilibration of the base line was performed by a continuous flow of 2% DMSO through the chip surface for $1 \sim 2$ h. WA was diluted into different concentrations with a constant DMSO concentration of 2%, and then injected into the protein binding channels at a flow rate of 10 ul/min followed by washing with the running buffer.

Molecular docking. The protein crystallographic structures were down-loaded from the Protein Data Bank. Protein Protocol in Discovery Studio 2.5 was used to prepare the protein. Molecular docking was performed with program GOLD version 3.0.1. During GOLD docking, the default parameters of genetic algorithm (GA) were applied to search reasonable binding conformation and ChemScore function was used to evaluate docking results.

Mouse xenograft model. The mouse-xenograft model was established by injection of 2×10^6 cells s.c. into the right armpit of 5-week old BALB/c male athymic mice (National Rodent Laboratory Animal Resource, Shanghai, China). The mice were randomized into 5 groups (6–7 mice per group): vehicle control (1% DMSO), 2.5 mg/kg Cisplatin, 20 mg/kg Cyclophosphamide and 5, 10, 20 mg/kg WA group when xenografts were palpable. Vehicle or drugs were administered intravenously everydays days until sacrifice; body weight and tumor size were measured and recorded at the same time. Tumor size was measured using electronic caliper, and the tumor volumes were calculated using the formula: length × width^2/2. On 20 days, mice were killed; tumors were collected, weighed, and photographed. Tumor inhibition effect was calculated using the following equation: tumor suppression (%) = (1-T/C) × 100, where T is the average tumor weight of the treated group and C is that of the control group. The institutional and national guidelines for the care and use of animals were followed and the Ethical Committee of the Second Military Medicine University approved the current study.

Immunohistochemical analysis. Tumors were harvested, fixed in 10% neutral buffered formalin at 4 °C for 24 h, and then embedded in paraffin. Tumor slides were deparaffinized and rehydrated using xylene and alcohol; for immunoperoxidase labeling, endogenous peroxidase was blocked with 3% H_2O_2 for 10 min at room temperature. Primary antibodies were reacted with the tissue overnight in a humid chamber at 4 °C and washed with PBS. Then slides were incubated with horseradish peroxidase-conjugated secondary antibodies for 1.5 h at 4 °C. Immunoreactive sites were visualized using 3,30-diaminobenzidine staining for 5 min. Sections were counterstained with hematoxylin, dehydrated and mounted with coverslips. The slides were viewed under a Nikon H500S microscope (Nikon Inc, Melville, NY, USA). For the immunohistochemical

quantification QC, five randomly images from each tumor were analyzed. The large necrotic areas in the xenograft were excluded from analysis.

Conflict of Interest

The authors declare no conflict of interest.

1. Siegel R, Ward E, Brawley O, Jemal A. Cancer Statistics, 2011: the impact of eliminating socioeconomic and racial disparities on premature cancer deaths. *CA Cancer J Clin* 2011; **61**: 212–236.
2. Reveiz L, Rueda JR, Cardona AF. Palliative endobronchial brachytherapy for non-small cell lung cancer. *Cochrane Database Syst Rev* 2012; doi:10.1002/14651858.CD004284.pub32012.
3. Voortman J, Lee JH, Killian JK, Suuriniemi M, Wang Y, Lucchi M et al. Array comparative genomic hybridization-based characterization of genetic alterations in pulmonary neuroendocrine tumors. *Pro Natl Acad Sci USA* 2010; **107**: 13040–13045.
4. Molina JR, Yang P, Cassivi SD, Schild SE, Adjei AA. Non-small cell lung cancer: epidemiology, risk factors, treatment and survivorship. *Mayo Clin Proc* 2008; **83**: 584–594.
5. Shen L, Li Z, Shen S, Niu X, Yu Y, Li Z et al. The synergistic effect of EGFR tyrosine kinase inhibitor gefitinib in combination with aromatase inhibitor anastrozole in non-small cell lung cancer cell lines. *Lung Cancer* 2012; **78**: 193–200.
6. Alamgeer M, Ganju V, Watkins DN. Novel therapeutic targets in non-small cell lung cancer. *Curr Opin Pharmacol* 2013; **13**: 394–401.
7. Sos ML, Dietlein F, Peifer M, Schöttle J, Balke-Want H, Müller C et al. A framework for identification of actionable cancer genome dependencies in small cell lung cancer. *Proc Natl Acad Sci USA* 2012; **109**: 17034–17039.
8. Downward J. Targeting RAS signalling pathways in cancer therapy. *Nat Rev Cancer* 2003; **3**: 11–22.
9. Cox AD, Der CJ. The dark side of Ras: regulation of apoptosis. *Oncogene* 2003; **22**: 8999–9006.
10. Woessmann W, Chen X, Borkhardt A. Ras-mediated activation of ERK by cisplatin induces cell death independently of p53 in osteosarcoma and neuroblastoma cell lines. *Cancer Chemother Pharmacol* 2002; **50**: 397–404.
11. Bacus SS, Gudkov AV, Lowe M, Lyass L, Yung Y, Komarov AP et al. Taxol-induced apoptosis depends on MAP kinase pathways (ERK and p38) and is independent of p53. *Oncogene* 2001; **20**: 147–155.
12. Tang D, Wu D, Hirao A, Lahti JM, Liu L, Mazza B et al. ERK activation mediates cell cycle arrest and apoptosis after DNA damage independently of p53. *J Biol Chem* 2002; **277**: 12710–12717.
13. Sun HF, Li XM, Meng L, Cui CM, Gao SS, Li CS et al. Asperolides A–C, tetranorlabdane diterpenoids from the marine alga-derived endophytic fungus Aspergillus wentii EN-48. *J Nat Prod* 2012; **75**: 148–152.
14. Lv C, Sun W, Sun H, Wei S, Chen R, Wang B et al. Asperolide A, a marine-derived tetranorditerpenoid, induces g2/m arrest in human nci-h460 lung carcinoma cells, is mediated by p53-p21 stabilization and modulated by ras/raf/mek/erk signaling pathway. *Mar Drugs* 2012; **11**: 316–331.
15. Zhang Z, Miao L, Lv C, Sun H, Wei S, Wang B et al. Wentilactone B induces G2/M phase arrest and apoptosis via the Ras/Raf/MAPK signaling pathway in human hepatoma SMMC-7721 cells. *Cell Death Dis* 2013; **4**: e657.
16. Zhang W, Liu HT. MAPK signal pathways in the regulation of cell proliferation in mammalian cells. *Cell Res* 2002; **12**: 9–18.
17. Vogelstein B, Lane D, Levine AJ. Surfing the p53 network. *Nature* 2000; **408**: 307–310.
18. Vousden KH, Lane DP. p53 in health and disease. *Nat Rev Mol Cell Biol* 2007; **8**: 275–283.
19. Wu GS. The functional interactions between the p53 and MAPK signaling pathways. *Cancer Biol Ther* 2004; **3**: 156–161.
20. Dulić V, Stein GH, Far DF, Reed SI. Nuclear accumulation of p21Cip1 at the onset of mitosis: A role at the G2/M-phase transition. *Mol Cell Biol* 1998; **18**: 546–557.
21. Benhar M, Engelberg D, Levitzki A. ROS stress-activated kinases and stress signaling in cancer. *EMBO Rep* 2002; **3**: 420–425.
22. Singh SV, Srivastava SK, Choi S, Lew KL, Antosiewicz J, Xiao D et al. Sulforaphane-induced cell death in human prostate cancer cells is initiated by reactive oxygen species. *J Biol Chem* 2005; **280**: 19911–19924.
23. Zhang R, Humphreys I, Sahu RP, Shi Y, Srivastava SK. In vitro and in vivo induction of apoptosis by capsaicin in pancreatic cancer cells is mediated through ROS generation and mitochondrial death pathway. *Apoptosis* 2008; **13**: 1465–1478.
24. McLean L, Soto U, Agama K, Francis J, Jimenez R, Pommier Y et al. Aminoflavone induces oxidative DNA damage and reactive oxidative species-mediated apoptosis in breast cancer cells. *Int. J. Cancer* 2008; **22**: 1665–1674.

25. Fleury C, Mignotte B, Vayssière JL. Mitochondrial reactive oxygen species in cell death signalling. *Biochimie* 2002; **84**: 131–141.
26. Kamata H, Hirata H. Redox Regulation of Cellular Signalling. *Cell Signal* 1999; **11**: 1–14.
27. de Rooij J, Bos JL. Minimal Ras-binding domain of Raf1 can be used as an activation-specific probe for Ras. *Oncogene* 1997; **14**: 623–625.
28. Kötting C, Kallenbach A, Suveyzdis Y, Wittinghofer A, Gerwert K. The GAP arginine finger movement into the catalytic site of Ras increases the activation entropy. *Proc Natl Acad Sci USA* 2008; **105**: 6260–6265.
29. Oren M. Regulation of the p53 tumor suppressor protein. *J Biol Chem* 1999; **274**: 36031–36034.
30. Ryan KM, Phillips AC, Vousden KH. Regulation and function of the p53 tumor suppressor protein. *Curr Opin Cell Biol* 2001; **13**: 332–337.
31. Banin S, Moyal L, Shieh S, Taya Y, Anderson CW, Chessa L *et al.* Enhanced phosphorylation of p53 by ATM in response to DNA damage. *Science* 1998; **281**: 1674–1677.
32. She QB, Chen N, Dong Z. ERKs and p38 kinase phosphorylate p53 protein at serine 15 in response to UV radiation. *J Biol Chem* 2000; **275**: 20444–20449.
33. Vaseva AV, Moll UM. The mitochondrial p53 pathway. *Biochim Biophys Acta* 2009; **1787**: 414–420.
34. Miyashita T, Harigai M, Hanada M, Reed JC. Identification of a p53-dependent negative response element in the bcl-2 gene. *Cancer Res* 1994; **54**: 3131–3135.
35. Miyashita T, Reed JC. Tumor suppressor p53 is a direct transcriptional activator of the human bax gene. *Cell* 1995; **80**: 293–299.
36. Mihara M, Erster S, Zaika A, Petrenko O, Chittenden T, Pancoska P *et al.* p53 has a direct apoptogenic role at the mitochondria. *Mol Cell* 2003; **11**: 577–590.
37. Chipuk JE, Kuwana T, Bouchier-Hayes L, Droin NM, Newmeyer DD, Schuler M *et al.* Direct activation of Bax by p53 mediates mitochondrial membrane permeabilization and apoptosis. *Science* 2004; **303**: 1010–1014.
38. Jiang P, Du W, Wu M. p53 and Bad: remote strangers become close friends. *Cell Res* 2007; **17**: 283–285.
39. Cuconati A, Mukherjee C, Perez D, White E. DNA damage response and MCL-1 destruction initiate apoptosis in adenovirus-infected cells. *Genes Dev* 2003; **17**: 2922–2932.
40. Xia Z, Dickens M, Raingeaud J, Davis RJ, Greenberg ME. Opposing effects of ERK and JNK-p38 MAP kinases on apoptosis. *Science* 1995; **270**: 1326–1331.
41. Eisenberg-Lerner A, Bialik S, Simon HU, Kimchi A. Life and death partners: apoptosis, autophagy and the cross-talk between them. *Cell Death Differ* 2009; **16**: 966–975.
42. Lowy DR, Willumsen BM. Function and regulation of Ras. *Annu Rev Biochem* 1993; **62**: 851–891.
43. Overmeyer JH, Maltese WA. Death pathways triggered by activated Ras in cancer cells. *Front Biosci* 2011; **16**: 1693–1713.
44. Davis MF, Vigil D, Campbell SL. Regulation of Ras proteins by reactive nitrogen species. *Free Radic Biol Med* 2011; **51**: 565–575.
45. Cherfils J, Zeghouf M. Regulation of small GTPases by GEFs, GAPs, and GDIs. *Physiol Rev* 2013; **93**: 269–309.
46. Rubio II, Wetzker R. A permissive function of phosphoinositide 3-kinase in ras activation mediated by inhibition of GTPase-activating proteins. *Curr Biol* 2000; **10**: R883.
47. Hofer F, Berdeaux R, Martin GS. Ras-independent activation of Ral by a Ca(2 +)-dependent pathway. *Curr Biol* 1998; **8**: 839–842.
48. Giaccone G. Clinical perspectives on platinum resistance. *Drugs* 2000; **59**: 37–38.
49. Stordal B, Davey M. Understanding cisplatin resistance using cellular models. *IUBMB Life* 2007; **59**: 696–699.

Supplementary Information accompanies this paper on Cell Death and Disease website (http://www.nature.com/cddis)